Mon. Not. R. Astron. Soc. **000**, 000–000 (0000) Printed 21 May 2014 (MN LATEX style file v2.2)

# Photospheric emission from long duration gamma-ray bursts powered by variable engines

Diego López-Cámara[1], Brian J. Morsony[2], Davide Lazzati[1,3⋆]
[1]*Department of Physics, NC State University, 2401 Stinson Drive, Raleigh, NC 27695-8202, USA*
[2]*Department of Astronomy, University of Wisconsin-Madison, 2535 Sterling Hall, 475 N. Charter Street, Madison WI 53706-1582, USA*
[3]*Department of Physics, Oregon State University, 301 Weniger Hall, Corvallis, OR 97331, USA*

arXiv:1404.5319v2 [astro-ph.HE] 20 May 2014

21 May 2014

**ABSTRACT**
We present the results of a set of numerical simulations of long-duration gamma-ray burst jets aimed at studying the effect of a variable engine on the peak frequency of the photospheric emission. Our simulations follow the propagation of the jet inside the progenitor star, its break-out, and the subsequent expansion in the environment out to the photospheric radius. A constant and two step-function models are considered for the engine luminosity. We show that our synthetic light-curves follow a luminosity-peak frequency correlation analogous to the Golenetskii correlation found in long-duration gamma-ray burst observations. Within the parameter space explored, it appears that the central engine luminosity profile does not have a significant effect on the location of a gamma-ray burst in the Luminosity-peak frequency plane, bursts from different central engines being indistinguishable from each other.

**Key words:** gamma-ray bursts: general — radiation mechanisms: thermal — hydrodynamics

## 1 INTRODUCTION

Ever since the detection of the first Gamma-ray burst (GRB) by Klebesadel et al. (1973) and with the increase of the number of observed GRBs it has been clear that many of them share some general characteristics and so have even been grouped together in sub-classification groups. For example, depending on their duration GRBs have been classified in either long or short (Kouveliotou et al. 1993). Strikingly, there are no two GRBs which are exactly the same as the other. Variability is commonly observed (Walker et al. 2000) in GRBs, and a significant fraction of the long GRBs ($\sim$85%) appear to be the result of several pulses (Borgonovo et al. 2007). The pre- and post-bursting activity, as well as dormant periods, still remain to be fully understood (Drago & Pagliara 2007). Fenimore & Ramirez-Ruiz (2000) discovered a correlation between the variability and the observed peak isotropic luminosity. Thus, it is noteworthy to study the effects that a pulsed central engine has on the prompt GRB emission.

The prompt emission of GRBs is characterized by bright, non-thermal spectra, peaking between a few tens of keV up to several MeV (Band et al. 1993; Kaneko et al. 2006; Gruber et al. 2014). The radiation mechanism responsible for the production of such emission is not fully understood, possibly owing to the great diversity of GRB spectra and light curves. Even though most proposed models are capable of finding a parameter set to fit any GRB spectrum, it has been so far impossible to make a synthesis and formulate a model that can successfully account for the diversity of the observations without requiring an adaptation to each individual burst, and resorting to extreme fine-tuning in some cases. An important tool in the effort of finding common properties among the diversity of burst observations is the sample of correlations among different bursts, such as the Amati, Yonetoku, and luminosity-Lorentz factor correlations (see Amati et al. (2002); Yonetoku et al. (2004); Ghirlanda et al. (2012) for further details, respectively).

In previous publications (Lazzati et al. 2011, 2013a) we have shown that the photospheric emission model for the prompt GRB emission can reproduce the Amati and luminosity-Lorentz factor correlations without requiring any fine tuning of parameters or any underlying correlation between the properties of the central engine and/or its relativistic outflow. Our simulations showed that the correlations are due to the most part to the observer angle effect: burst seen close to their jet axes appear brighter, have a higher peak frequency, and are produced by faster ejecta compared to bursts observed near the edge of their jets. One lingering uncertainty was, however, the robustness of the observational correlations that we attempted to explain. A significant amount of work has been carried out in trying to establish the role of selection effects in the Amati and Yonetoku correlations, with contradictory results, at best (Band & Preece 2005; Nakar & Piran 2005; Ghirlanda et al. 2008; Butler et al. 2009; Krimm et al. 2009; Kocevski 2012; Heussaff et al. 2013). A more robust correlation that is certainly not affected by selection effects is the Golenetskii correlation, discovered by the Konus experiment (Golenetskii et al. 1983) and

⋆ E-mail:lazzatid@science.oregonstate.edu

confirmed more recently with the high-quality Fermi spectral data (Ghirlanda et al. 2010; Lu et al. 2012). According to the Golenetskii correlation, different time intervals of a single burst aligned along a straight line when plotted in the luminosity-peak frequency plane (for further discussion see Bhat et al. (1994); Borgonovo & Ryde (2001); Ford et al. (1995); Kargatis et al. (1994); Lu et al. (2010); Norris et al. (1986); Peng et al. (2009). The burst spectrum peaks at lower frequencies when the emission is weak but moves to higher frequencies when it is bright. In order to study whether photosphere-dominated bursts obey this correlation, we have carried out three hydrodynamic simulations of relativistic jets from collapsars. Two have engines with highly variable energy output while the third, the control, has a constant engine, analogously to our previous work (Morsony et al. 2010). We note that the fact that photosphere-dominated GRBs obey the Amati correlation does not imply that they should be able to reproduce the Golenetskii correlation. As a matter of fact, we showed that the difference in viewing angle is fundamental in producing the Amati correlation within the photospheric scenario (Lazzati et al. 2011, 2013a). In the Golenetskii case, instead, the viewing angle cannot play any role, since the observer is the same throughout the burst. This paper is organized as follows. We first describe the initial setup, and the numerical models in Section 2, followed by discussion of the the morphology, photospheric, and observable correlation's from our models in Section 3.. Conclusions are given in Section 4.

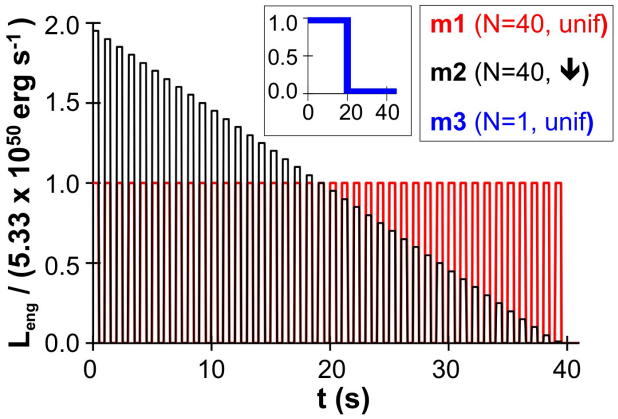


**Figure 1.** Engine luminosity for models m1 (red line), m2 (black line), and m3 (blue line).

## 2 INITIAL SETUP AND NUMERICAL MODELS

A variable relativistic two-dimensional (2D) jet was followed as it drilled through the stellar progenitor, and then as it evolved through an extremely large interstellar (ISM) domain. The jet was followed at all times with comparable resolution ($\Delta$=8$\times$10$^6$ cm) as in two-dimensional previous studies (Zhang et al. 2003, 2004; Morsony et al. 2007, 2010; Lazzati et al. 2009, 2012; Nagakura et al. 2011; Mizuta & Ioka 2013), in a domain large enough to be able to include the radius at which the spectrum is formed ($R_{sp}$ $\sim$10$^{12}$ cm). The spectrum formation radius is smaller than the photospheric radius, at which the Thomson scattering opacity equals unity (Giannios 2012). In order to solve correctly the transition between the active and quiescent epochs, the cocoon (region which surrounds the jet and which is conformed by a mixture of shocked jet and shocked stellar material (Ramirez-Ruiz et al. 2002; Lazzati & Begelman 2005)) was solved with a much finer resolution ($\Delta$=3.2$\times$10$^7$ cm) than the previous numerical studies. In order for the domain to include the spectral radius $R_{\rm sp}$, the simulation box was 2.56$\times$10$^{12}$ cm in length (along the jet direction) and 5.12$\times$10$^{11}$ cm across. The difference between the finest resolution level and the size of the domain (5 orders of magnitude), combined with the necessary integration time for the jet to reach $R_{\rm sp}$ ($\sim$100 s), required the use of an adaptive mesh code. Thus, we used the Flash code (version 2.5) (Fryxell et al. 2000).

The numerical setup, physics, and assumptions in this study were, unless stated differently, the same as those in (Lazzati et al. 2013a). The stellar progenitor, model 16TI from (Woosley & Heger 2006), was immersed in a interstellar medium with constant density ($\rho_{\rm ism}$=10$^{-13}$ g cm$^{-3}$). The variable jet was launched from the core of the progenitor and depending on the model was followed for a total integration time between 110 and 135 seconds. This time was long enough for the jets to break out of the progenitor, evolve through the ISM, and cross entirely the $R_{\rm sp}$. The jet had at all times a half-opening angle $\theta_0$=10$^o$ at injection, an initial Lorentz Factor $\Gamma_0$=5, and a ratio of internal over rest-mass energy $\eta_0$=80. Even though it would be important to check the dependence of the results on all these parameters, as well as on the progenitor mass and structure, the challenging nature of the simulations prevented us from performing a thorough study of the parameter dependencies. The overall activity time of the central engine was set taking into account that the width of the observed duration of long BATSE gamma-ray bursts is mostly accounted for by an engine lasting 20 s (Lazzati et al. 2013b). The variable temporal behavior of the jet consisted of a series of N step functions (all with the same "on" and "off" durations, $\delta t$) before the engine luminosity was suddenly decreased to a negligible value and eventually turned off when the maximum integration time was reached. The two models consisted of forty half-second episodes before the engine was turned off. The active stages of the first model (m1) had a luminosity equal to $L_0 = 5.33\times10^{50}$ erg s$^{-1}$, while the quiescent stages were three orders of magnitude dimmer. The second model (m2) had a monotonically decreasing step function distribution for the value of the luminosity of the pulses. In order for both models to have the same overall energy the initial pulse of model m2 had luminosity $1.95L_0$, each subsequent pulse diminished 5% until the final pulse had luminosity $0.05L_0$. In addition, we ran an extra simulation with a single twenty second active period before the jet was turned off (model m3, our control case). The characteristics of our models are shown in Figure 1. We must note that this study was two-dimensional and one could expect that there would be significant changes in three-dimensions. However, two-dimensional simulations are much less demanding in terms of CPU hours and these simulations could not be performed in 3D. A comparison between 2 and 3D simulations on smaller domains showed that 2D simulations give reliable results since the overall jet behavior is only marginally affected by the dimensionality. López-Cámara et al. (2013) show that the overall morphology and large-scale features of 2D GRB jets resemble those from three-dimensional, even though 2D jet models break out at later times and present less turbulence.

## 3 RESULTS AND DISCUSSION

### 3.1 Global morphology.

Before we discuss the morphology, evolution, and photospheric emission of the episodic jet, we first describe our control case (model m3), the single 20 second spike model. The results for the single spiked model were consistent with the results obtained from previous two- (Zhang et al. 2003, 2004; Morsony et al. 2007, 2010; Mizuta & Ioka 2013), and three-dimensional GRB-jet studies (López-Cámara et al. 2013), as well as within the breakout time range of Bromberg et al. (2011) analytical model. The 20 second single pulse model drills through the stellar envelope and breaks out of the progenitor (see the three right panels from Figure 2). The forward, reverse, collimation and oblique shocks are present, and the break out time was $t_{\rm bo}$=6.8 s. We must point out that due to the fact that we have a finer cocoon resolution, the breakout time of our control case is slightly longer than that seen for example in (Morsony et al. 2010). The jet is at all times low-density ($\rho \sim 10^{-3}$ g cm$^{-3}$), and before the jet breaks out of the star it is mildly relativistic. The regions where the collimation and oblique shocks are present reach $\Gamma$ values close to $\sim$ 10 within seconds (see the schematic Figure 3 from Mizuta & Ioka (2013) for more details). Before the jet breaks out of the star, these regions reach values close to $\Gamma \sim$20. Once the jet breaks out of the star it reaches $\Gamma \sim$130 (at $Z_{\rm obs}$).

Each pulse from the step jet models (m1 and m2) were low-density at all times ($\rho \sim 10^{-3}$ g cm$^{-3}$) and mildly relativistic before the break out ($\Gamma \sim$10). The quiescent periods between the pulses, on the other hand, were at least two orders of magnitude denser than the pulses and were sub-relativistic. The break out time for model m1 and m2 was $t_{\rm bo}$=10.7 s and 7.8 s, respectively. Note that the break out time decreases monotonically with increasing average engine luminosity, as expected. For both episodic models, a set of the initial pulses is destroyed by the dense stellar envelope before the jet is able to brake out of the progenitor. For model m1 (m2) the first nine (seven) pulses are destroyed. In order to clarify this the destruction of one of the pulses is shown in the two left panels from Figure 2. Notice how the fifth pulse from model m1 (present at 5.5 s) disappears before the next pulse is even launched. Each time a pulse was engulfed by the stellar envelope, the subsequent pulse managed to drill further out of the star and, unless it reached the stellar surface, it would also be destroyed. Once the jet brakes out of the star, the pulse destruction ceased to occur. This is further clarified by the middle panels of Figure 2. In these, when $t = 10.7$ s the tenth pulse from model m1 is not destroyed and reaches the stellar surface. The subsequent pulses also break out of the star. For example, the eleventh pulse (situated at $\sim 10^{10}$ cm at 10.7s) when $t = 12.1$ also breaks out of the progenitor. A similar behavior was observed in simulations of a rapidly varying jets studied by Morsony et al. (2010). There, jets with 0.1s pulses and random power variability on 0.1 s timescales were used. In both cases, the first few seconds of jet variability were wiped out by strong interaction with the stellar envelop as the jet propagated. At later times, however, there was a strong correspondence between the input variability of the central engine and the short time scale variability of the jet seen at large radii. It is noteworthy to mention that if the quiescent period between pulses was too large, then the pressure from the stellar envelope would fill the funnel that the recently destroyed pulse had created. For the chosen progenitor, if the dormant epochs lasted more than one second then the funnel would always collapse and the jet propagation would be hindered.

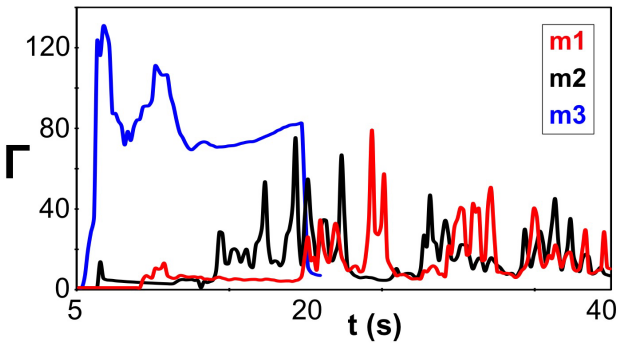


**Figure 4.** Temporal Lorentz factor evolution at $Z_{\rm obs}$ for models m1 (black), m2 (red), and m3 (blue).

The evolution of the variable jet through the ISM is illustrated in Figure 3. In this, the density and $\Gamma$ stratification maps for model m1 at different times are shown. Both models broke out of the star, and the episodic jets reach $Z_{\rm obs}$ after approximately 100 s. Akin to the single spike, before the break up time the active periods have $\rho \sim 10^{-3}$ g cm$^{-3}$ and $\Gamma \sim$15. We must state that model m2 had an overall evolution similar to that of m1. It mainly differs in the fact that, since the initial pulses were more energetic than those from m1, it broke out of the progenitor and reached $Z_{\rm obs}$ faster than for m1. Also, as the control model, once $t > t_{\rm bo}$ the active periods accelerate while decreasing their density. The pulses reach values as low as $\rho \sim 10^{-6}$ g cm$^{-3}$ (the quiescent epochs remain two orders of magnitude lower), and Lorentz factors as high as $\Gamma$=80 (quiescent periods as expected have $\Gamma \sim$1).

In order to illustrate the relativistic motion of the pulses, Figure 4 shows the temporal evolution of $\Gamma$ for an observer set at $Z_{\rm obs}$ with a $\theta$=1$^o$ viewing angle. The single pulse model initially reaches a Lorentz factor value close to 120 and after $\sim$10 s remains fairly constant with $\Gamma \sim$80. On the other hand, the episodic jet models behavior is clearly present at $Z_{\rm obs}$ and oscillates between $\Gamma = 10 - 80$. The $\Gamma$ temporal structure for different viewing angles for the episodic models also shows this variability, but the maximum Lorentz values are noticeably lower (e.g. 56 and 34 for model m1 seen at $Z_{\rm obs}$ with 3$^o$ and 5$^o$ viewing angle, respectively).

### 3.2 Photospheric light curves

Giannios (2012) has shown that the spectrum in a relativistic outflow is formed inside the photosphere, when the scattering optical depth reaches a critical value

$$\tau_T = 46 \frac{L_{53}^{1/6} f_{\pm}^{1/3}}{\Gamma_{2.5}^{1/3} \epsilon^{1/6} \eta_{2.5}^{1/3}} \quad (1)$$

The location of the critical optical depth is found by computing the optical depth backward in space and time from an imaginary observed located at $Z_{\rm obs} = 2.5 \times 10^{12}$ cm from the center of the explosion. Retarded time and the effect of the relativistic expansion of the fluid are taken into account by enforcing (Lazzati et al. 2013a):

$$46 \frac{L_{53}^{1/6} f_{\pm}^{1/3}}{\Gamma_{2.5}^{1/3} \epsilon^{1/6} \eta_{2.5}^{1/3}} =$$
$$= - \int_{Z_{\rm obs}}^{Z_{\rm sp}(x)} \sigma_T n' \left( t_{\rm obs} - \frac{Z_{\rm obs} - z}{c}, x, z \right) \Gamma \left[ 1 - \beta \cos(\theta_v) \right] dz \quad (2)$$

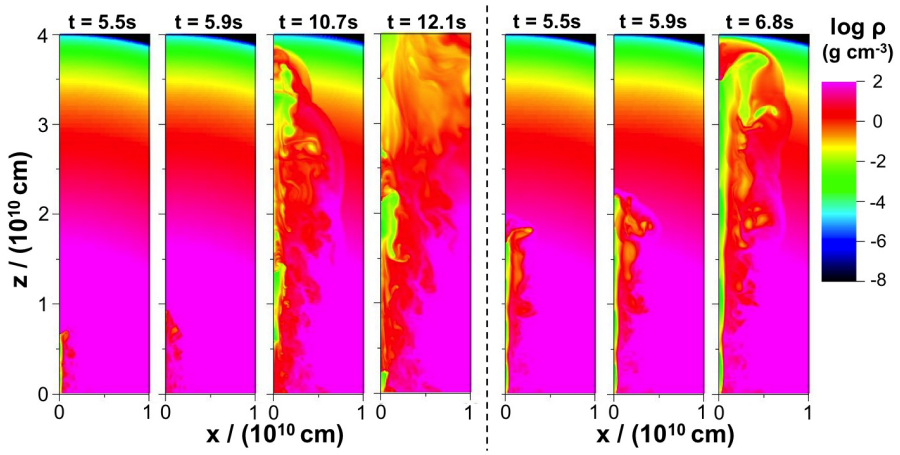


**Figure 2.** Density (g cm$^{-3}$) stratification maps for model m1 (4 left panels), and for model m3 (3 right panels) at different times.

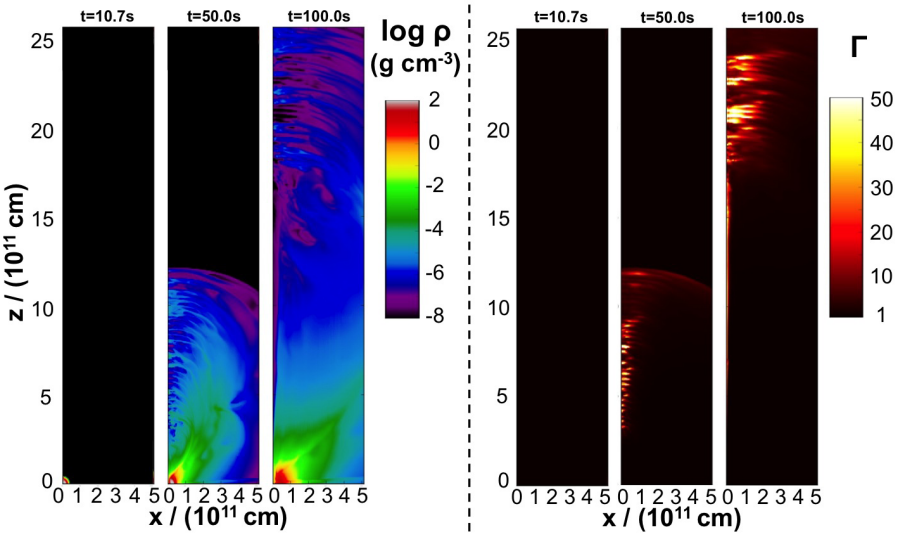


**Figure 3.** Density (g cm$^{-3}$) stratification maps (3 left panels), and Lorentz factor maps (3 right panels) for model m1.

where $\beta \equiv \beta(t_{\rm lab}, x, z)$ is the local velocity of the outflow in units of the speed of light, $\Gamma \equiv \Gamma(t_{\rm lab}, x, z)$ is the local bulk Lorentz factor, and $\theta_v \equiv \theta_v(t_{\rm lab}, x, z)$ is the angle between the velocity vector and the direction of the line of sight. $x$ is the coordinate perpendicular to the line of sight, while $z$ is the coordinate along the line of sight[1]. All the values of $\beta$, $\Gamma$, and $\theta_v$ are evaluated at the same delayed coordinate $(t_{\rm lab}, x, z) \equiv \left(t_{\rm obs} - \frac{Z_{\rm obs}-z}{c}, x, z\right)$ as the comoving density.

Once the location of the spectral radius is found, we compute the bolometric luminosity and the peak frequency of the emission following Lazzati et al. (2013a). We stress that we do not compute the whole spectral shape of the burst, since that would require detailed radiation transfer calculations beyond the scope of this research. The resulting light curves are shown in Figure 5.

The variable behavior of models m1 and m2, as well as the observer viewing angle, have direct impact on the photospheric light curves. The photospheric light curve of the pulsed models also has an episodic behavior. Though there is not a clear one to one relationship between the launched pulses (shown in Figure 1) and the spikes in the light curve (shown in Figure 5), it is clear that the half second pulses produce ≈1 s episodes, a time lapse which is actually the typical pulse width observed in the light curves of variable long GRBs (Fenimore et al. 1995; Norris et al. 1996), and with the luminosity ranging from $10^{52}$erg s$^{-1}$ to $4\times10^{53}$erg s$^{-1}$. This behavior is clearly not present in the single 20 s pulse. The episodic temporal evolution is present independently of the viewing angle, but as expected the luminosity decreases for larger viewing angles. For example, for a $3^o$ viewing angle the maximum value of the photospheric luminosity is $2\times10^{53}$erg s$^{-1}$, and $8\times10^{52}$erg s$^{-1}$ for when the viewing angle is $5^o$ (see middle and lower panels from Figure 5 respectively). The different temporal distributions with which the pulses from model m1 (pulses all with the same luminosity) and m2 (pulses with a linearly decreasing step function luminosity) were launched are not immediately recognizable in the photospheric luminosity. We computed the power spectra of all light curves. The power spectra of the variable models (m1 and m2) are indistinguishable from each other at all viewing angles,

[1] Note that, strictly speaking, we do not find the spectral radius but the z-coordinate of the location at which the spectrum is formed. This allows us to implicitly take into account the equal arrival time surfaces.

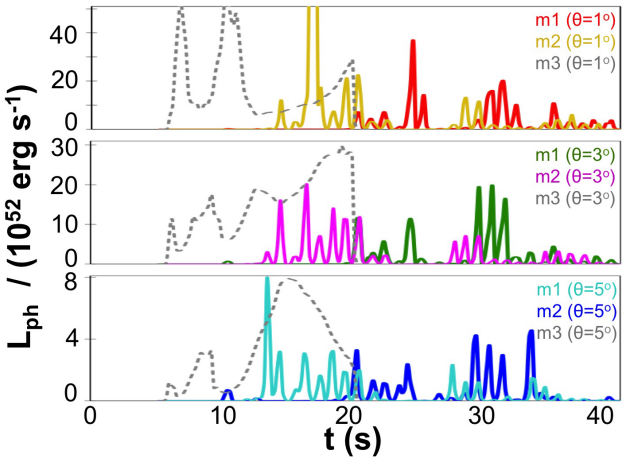


**Figure 5.** Photospheric light curves of the three models at different viewing angles (top panel is for $\theta$=1$^o$, middle panel $\theta$=3$^o$, and bottom panel $\theta$=5$^o$).

with a red noise component that can be modeled as a $\nu^{-2}$ power law plus a marked periodicity at 1 Hz. This is not surprising since the engine is strictly periodic with a 1 s period (fast variability is known to propagate with the jet unaffected by the star: Morsony et al. (2010)). The non-variable model (m3) has a similar behavior but does not have any periodic signal. The power spectra of models m1 and m2 (the variable ones) are not consisted with observed GRBs, since observed light curves do not have any periodicity. However, given the lack of an easy recipe for simulating a GRB light curve, any choice of the engine luminosity profile would be as questionable as any other. We adopted a periodic input in order to limit the degrees of freedom in the choice of the engine variability.

### 3.3 The Golenetskii correlation

The peak frequency ($E_{\rm pk}$) and corresponding isotropic luminosity ($L_{\rm iso}$) were calculated for every half second interval in which the engine was active. To better reproduce observations, where the peak frequency is computed by time integrating the spectrum over the interval, we report the luminosity-weighted average peak frequency:

$$\langle h\nu_{\rm pk}\rangle_{\rm int} = h\frac{\int_t^{t+\delta t} L(t)\nu_{\rm pk}(t)\,dt}{\int_t^{t+\delta t} L(t)\,dt} \qquad (3)$$

The resulting relationship between the peak frequency and luminosity for each burst, as well as the Amati relationship are shown in Figure 6. The observational correlation between peak frequency and luminosity was discovered by Golenetskii et al. (1983) and is also known as the internal Yonetoku correlation (i.e. the Yonetoku correlation for individual bursts, Yonetoku et al. 2010). We show the observed best fit correlation with a solid line (Lu et al. 2012) and we delimit the 2-sigma confidence region with dashed lines. For all three models the data from the synthetic light curves and spectra show agreement with the observations. As can be seen in Figure 6 the majority of the dataset we obtain is within the two-sigma confidence region. Specifically, the Golenetskii relationship for the whole dataset (log($E_{\rm pk}$=-28.60$\pm$1.40)+(0.59$\pm$0.03)) is very similar to that from the bright variable GRB dataset observed by Fermi (Lu et al. 2012) (log($E_{\rm pk}$=-29.854$\pm$0.178)+(0.621$\pm$0.003)). However, when the models are considered individually, the agreement weakens. For example, the average correlations for all viewing angles of the three models presented are: log($E_{\rm pk}$=-20.60$\pm$2.10)+(0.44$\pm$0.04), log($E_{\rm pk}$=-24.10$\pm$2.50)+(0.50$\pm$0.05), and log($E_{\rm pk}$=-35.30$\pm$3.00)+(0.70$\pm$0.06) for m1, m2, and m3, respectively.

The synthetic data populate the region in the lower right of the observed correlation and are therefore typical of a burst that is somewhat "soft" for the given luminosity. In the inset of Figure 6 we show where the time-integrated pulsed bursts would lie in the Amati plane. Such bursts populate the lower right part of the Amati correlation and are also within the two-sigma confidence region. The Amati relationship obtained ($E_{\rm pk}$=(3.3 $E_{iso,52}^{0.79}$)) is quite steeper than the Amati et al. (2002) relationship ($E_{\rm pk}$=(118 $E_{iso,52}^{0.486}$)). The fact that the simulated bursts populate the lower right portion of the Amati and Golenetskii correlations is worth further investigation. A previous set of simulations of constant engine GRBs showed quantitative agreement with the Amati correlation (Lazzati et al. 2013a). At this stage, it is unclear if the difference is due to the different numerical setup or to the somewhat extreme variability adopted in this paper, with the engine shutting off for half a second periods regularly. We are planning to perform a more thorough study of variable jets with different variability properties and inside different progenitors to ascertain if the cause of the softness is intrinsic, numerical, or related to the particular parametrization of the jet/star pair used in this paper. One important note about Figure 6 is that the graph shows only the properties of the bright pulses, i.e., those with a peak luminosity larger than 1 per cent of the brightest peak. This choice was motivated by the fact that observationally only the brightest part of a burst is amenable to time-resolved spectral analysis and can be shown in the Golenetskii plane. Since simulated light curves have no noise, we can measure luminosity and peak frequencies for the weakest burst intervals. Interestingly, these intervals deviate from the correlation shown in the figure adding a flatter tail, lying above the correlation, in the range of luminosities $10^{48} < L_{\rm iso} < 10^{50}$ erg/s. It is unclear at this moment whether this is a model prediction or an artifact of the simulations. As a matter of fact, time intervals with low-luminosity are characterized by an enhanced baryon loading in the outflow and our spectral calculations are not fully trustable when the location of the spectral radius approaches the edge of the simulation domain.

## 4 SUMMARY AND CONCLUSIONS

We presented the results of a set of numerical simulations of long-duration GRB jets followed as they propagate through their progenitor star, reach break-out, and expand outward until reaching the radius at which the spectrum of the advected radiation converge to a constant shape to be eventually released at the photosphere. This is the first time that jets from engines with variable luminosity are studied in such an extended domain. Our simulations allow us to explore whether the photospheric emission of jets from unsteady engines follows the Golenetskii correlation between the time-resolved luminosity and spectral peak.

We find that the synthetic light curves and spectra from our three models reproduce the Golenetskii and Amati correlations, lending more support to the scenario in which the bulk of the burst prompt radiation is advected in the outflow and released at the photosphere. One notable exception is the light curve for an on-axis observer in our control model (m3). In that case, the synthetic datapoint for an horizontal line that does not follow the Golenetskii

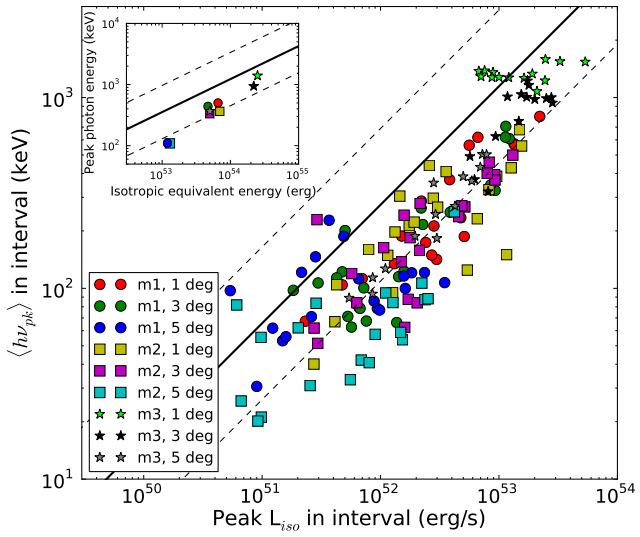


**Figure 6.** Synthetic Golenetskii correlation for models m1, m2 and m3 at various viewing angles, as indicated in the legend. The solid line represent the best fit of Fermi data (Lu et al. 2012) and their 2-sigma confidence (dashed lines). The inset show the synthetic bursts on the Amati plane.

correlation. It appears, therefore, that while all GRBs from variable engines obey the correlation, outliers can be produced by engines of constant luminosity. Our simulations attempted to reproduce the correlation as a pulse-by-pulse phenomenon. The engine was set up to produce short pulses of half a second. Half a second features were detected in the light curves and analyzed as pulses, each pulse providing a single point in the Golenetskii plane. Observationally, the latter correlation is detected also within pulses, i.e., when the signal to noise is so high that a pulse can be split in sub-intervals. Our simulations cannot address this situation, at present. A new set of simulations with longer pulses and higher temporal resolution is planned and will be presented in a future publication.

**Acknowledgements** We would like to thank the anonymous referee for constructive suggestions that led to the improvement of this paper. We thank S.E. Woosley and A. Heger for making their pre-SN models available. The software used in this work was in part developed by the DOE-supported ASC/Alliance Center for Astrophysical Thermonuclear Flashes at the University of Chicago. This work was supported in part by the Fermi GI program grant NNX12AO74G and Swift GI program grant NNX13A095G (DL and DLC). BJM is supported by an NSF Astronomy and Astrophysics Postdoctoral Fellowship under award AST-1102796.

## REFERENCES

Amati, L., Frontera, F., Tavani, M., et al. 2002, A&A, 390, 81
Band, D., Matteson, J., Ford, L., et al. 1993, ApJ, 413, 281
Band D. L., Preece R. D., 2005, ApJ, 627, 319
Bhat, P. N., Fishman, G. J., Meegan, C. A., et al. 1994, ApJ, 426, 604
Borgonovo, L., Frontera, F., Guidorzi, C., et al. 2007, A&A, 465, 765
Borgonovo, L., & Ryde, F. 2001, ApJ, 548, 770
Bromberg, O., Nakar, E., Piran, T., & Sari, R. 2011, ApJ, 740, 100
Butler N. R., Kocevski D., Bloom J. S., 2009, ApJ, 694, 76
Drago, A., & Pagliara, G. 2007, ApJ, 665, 1227
Fenimore, E. E., in 't Zand, J. J. M., Norris, J. P., Bonnell, J. T., & Nemiroff, R. J. 1995, ApJL, 448, L101
Fenimore, E. E., & Ramirez-Ruiz, E. 2000, arXiv:astro-ph/0004176
Ford, L. A., Band, D. L., Matteson, J. L., et al. 1995, ApJ, 439, 307
Fryxell, B., Olson, K., Ricker, P., et al. 2000, ApJs, 131, 273
Ghirlanda G., Nava L., Ghisellini G., Firmani C., Cabrera J. I., 2008, MNRAS, 387, 319
Ghirlanda G., Nava L., Ghisellini G., 2010, A&A, 511, A43
Ghirlanda, G., Nava, L., Ghisellini, G., et al. 2012, MNRAS, 420, 483
Giannios, D. 2012, MNRAS, 422, 3092
Golenetskii, S. V.,Mazets, E. P., Aptekar, R. L., & Ilinskii, V. N. 1983, Nature, 306, 451
Gruber D., et al., 2014, ApJS in press (arXiv:1401.5069)
Heussaff V., Atteia J.-L., Zolnierowski Y., 2013, A&A, 557, A100
Kaneko, Y., Preece, R. D., Briggs, M. S., et al. 2006, ApJS, 166, 298
Kargatis, V. E., Liang, E. P., Hurley, K. C., et al. 1994, ApJ, 422, 260
Klebesadel, R. W., Strong, I. B., & Olson, R. A. 1973, ApJL, 182, L85
Kocevski D., 2012, ApJ, 747, 146
Kouveliotou, C., Meegan, C. A., Fishman, G. J., et al. 1993, ApJL, 413, L101
Krimm H. A., et al., 2009, ApJ, 704, 1405
Lazzati, D., & Begelman, M. C. 2005, ApJ, 629, 903
Lazzati, D., Morsony, B. J., & Begelman, M. C. 2009, ApJl, 700, L47
Lazzati, D., Morsony, B. J., & Begelman, M. C. 2011b, ApJ, 732, 34
Lazzati, D., Morsony, B. J., Blackwell, C. H., & Begelman, M. C. 2012, ApJ, 750, 68
Lazzati, D., Morsony, B. J., Margutti, R., & Begelman, M. C. 2013, ApJ, 765, 103
Lazzati, D., Villeneuve, M., Lopez-Camara, D., Morsony, B., & Perna, R. 2013, arXiv:1309.1473
López-Cámara, D., Morsony, B. J., Begelman, M. C., & Lazzati, D. 2013, ApJ 767, 19
Lu, R.-J., Hou, S.-J., & Liang, E.-W. 2010, ApJ, 720, 1146
Lu, R.-J., Wei, J.-J., Liang, E.-W., et al. 2012, ApJ, 756, 112
Mizuta, A., & Ioka, K. 2013, ApJ, 777, 162
Morsony, B. J., Lazzati, D., & Begelman, M. C. 2007, ApJ, 665, 569
Morsony, B. J., Lazzati, D., & Begelman, M. C. 2010, ApJ, 723, 267
Nagakura, H., Ito, H., Kiuchi, K., & Yamada, S. 2011, ApJ, 731, 80
Nakar E., Piran T., 2005, MNRAS, 360, L73
Norris, J. P., Nemiroff, R. J., Bonnell, J. T., et al. 1996, ApJ, 459, 393
Norris, J. P., Share, G. H., Messina, D. C., et al. 1986, ApJ, 301, 213
Peng, Z. Y., Ma, L., Zhao, X. H., et al. 2009, ApJ, 698, 417
Ramirez-Ruiz E., Celotti A., Rees M. J., 2002, MNRAS, 337, 1349
Walker, K. C., Schaefer, B. E., & Fenimore, E. E. 2000, ApJ, 537, 264
Woosley S. E., & Heger A. 2006, ApJ, 637, 914

Yonetoku, D., Murakami, T., Nakamura, T., et al. 2004, ApJ, 609, 935
Yonetoku, D., Murakami, T., Tsutsui, R., et al. 2010, Publications of the Astronomical Society of Japan, 62, 1495
Zhang, W., Woosley, S. E., & Heger, A. 2004, ApJ, 608, 365
Zhang, W., Woosley, S. E., & MacFadyen, A. I. 2003, ApJ, 586, 356